BOUNDARY SHEAR STRESS DISTRIBUTION IN RECTANGULAR OPEN CHANNELS

BY N. RAJARATNAM *
AND D. MURALIDHAR *

Introduction

A knowledge of the distribution of the boundary shear stress in open channels is necessary not only for the economical designing of water courses but also for understanding the mechanics of turbulent flow in these channels. Leighly [1] and Lane [2, 3] obtained the shear stress distribution for certain channel shapes by dividing the area into sub-areas bounded by orthogonals to the isovels. Lundgren and Jonsson [4] developed a method for shallow channels with rough beds. Ippen et al. [5] measured the stress distribution in trapezoidal channels, in the course of their work on flow in channel bends, using the Preston tube [6]. Enger [7] computed the shear stress distribution for some trapezoidal sections with erodible boundaries assuming a certain velocity distribution equation.

Recently Cruff [8] has obtained considerable experimental data for smooth rectangular channels. In some cases, the shear stress was measured with a Preston tube and in the remaining cases they were computed using the well known Prandtl-Karman logarithmic velocity distribution equation. Replogle and Chow [9] measured the shear stress distribution in circular channels using the Preston method. Some shear stress measurements for rectangular channels have also been reported by Davidian and Cahal [10].

This paper presents some more measurements on the shear stress distribution in smooth rectangular channels. Further the maximum stresses on the bed and sides have been correlated with the results of the boundary layer theory. A relation has been obtained connecting the maximum wall shear stress with the bed shear stress in an infinitely wide channel. Further the boundary layers on the bed and sides have been studied regarding the velocity distribution. Some interesting results have been obtained regarding the velocity dip at the free surface and the discharge distribution. Only supercritical flows have been considered in this work. The Froude number of the flows varied from about 1.1 to about 2.4. In the entire range of Froude numbers studied, there was no perceptible formation of roll waves [11]. The subcritical studies have not been successful so far due to difficulties with the velocity and shear measuring instruments for low velocities.

Experimental arrangements and experiments

The experiments were done in two rectangular channels. The first channel was a smooth channel with the bed and sides made of plexiglass. It had a width of nine inches, depth of eight inches and length of 32 feet with an adjustable slope. Water entered the flume from a constant head tank provided with suitable screens. The discharge Q was measured by means of an orifice-meter located in the supply line to the constant head tank.

The water surface profile in the flume was measured by means of piezometers located in the bed of the flume. The test section was located at a distance of about 24 feet from the entrance section. Velocities were measured using a 3 mm external dia-

* N. Rajaratnam, Associate Professor; D. Muralidhar, Research Associate. Department of Civil Engineering, University of Alberta, Edmonton, Alberta, Canada.

meter Prandtl-type Pitot static tube. The same Prandtl tube was also used as a Preston tube [12, 13].

Six experiments (1 A — 1 F) were done in this channel. If V is the mean velocity of flow and y_0 is the normal depth, then the Froude number, defined as $\mathcal{F} = V/\sqrt{gy_0}$, where g is the acceleration due to gravity, was varied from 1.25 to 2.31. Velocity and the boundary shear stress distributions were obtained in one half of the channel. Figure 1 shows a typical velocity distribution where u is the velocity at a normal distance of y above the bed and z denotes the transverse distance from the centerplane of the channel. If $\lambda = z/(b/2)$, where b is the breadth of the channel, for λ from zero up to about 0.89, u varies linearly with log y and for $\lambda \simeq 1.0$, the variation becomes curvilinear. (No corrections have been made to the velocity measurements for the Pitot displacement, turbulence and other effects.) Further, Figure 1 shows that there is a dip

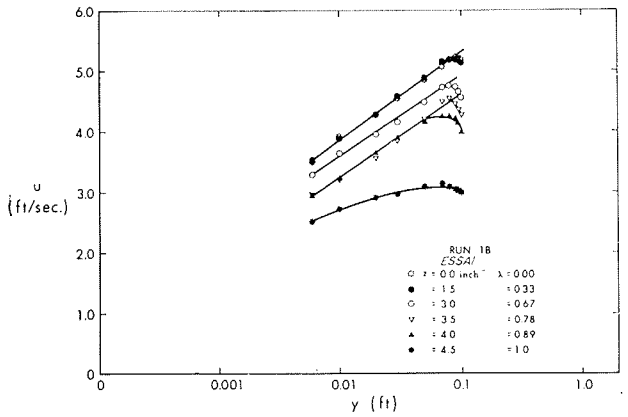

1/ Typical velocity distribution.
Répartition-type des vitesses.

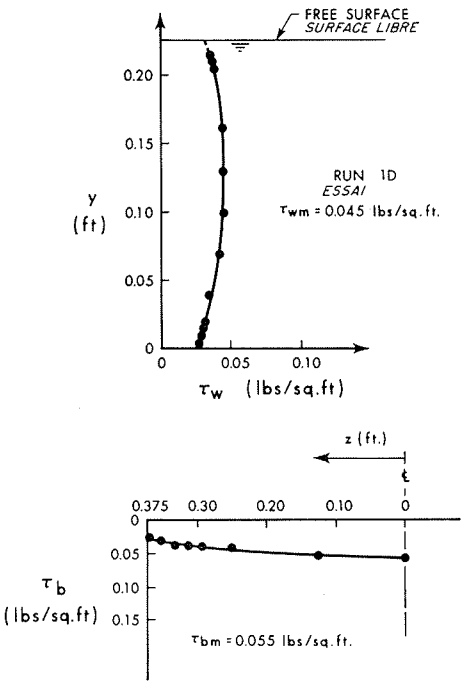

2/ Typical boundary shear stress distributions.
Répartition-type de la contrainte de cisaillement aux limites.

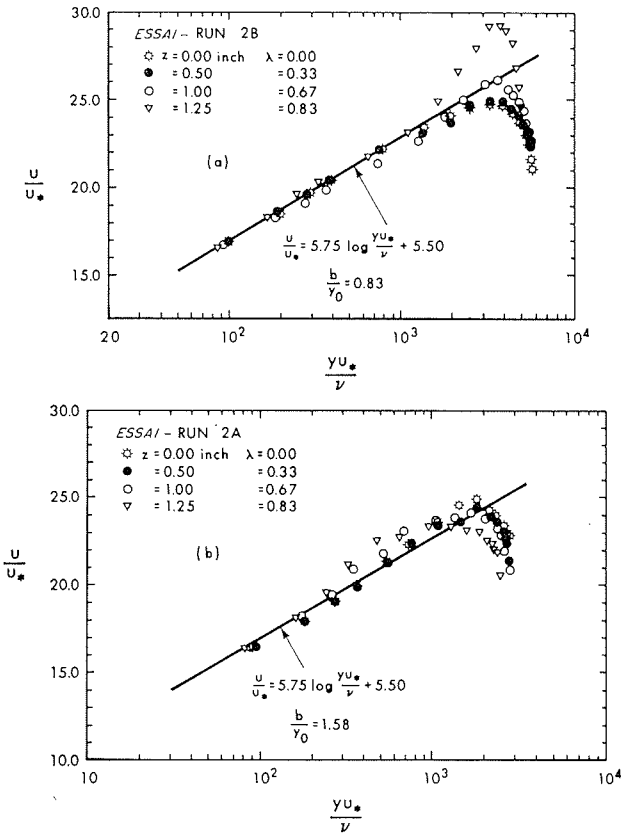

3/ Velocity distributions for various aspect ratios (a to f).
Répartition des vitesses en fonction de l'allongement (a à f).

in the velocity distribution in the neighbourhood of the free surface. This aspect is discussed later on.

Figure 2 shows a typical boundary shear stress distribution on the bed and side walls as obtained by the Preston tube technique. From a study of Figure 2 and the results for the other experiments, it was found that in general, the boundary shear stress on the bed τ_b has a maximum value of τ_{bm} on the centerline of the bed and decreases as the wall is approached. On the side wall, the shear stress τ_w increases with the distance y from the bed up to some value of y, then remains constant at a maximum value of τ_{wm} for a certain depth and exhibits a decrease as the free surface is approached.

For the second series of two experiments, the width of the plexiglass channel was reduced to 3.0 inches by the introduction of a box-like unit with a smooth plywood side. In these two series, the aspect ratio b/y_0 has been varied from 0.83 to 10.82.

The third series of experiments were done in a large rectangular channel of width of 2.94 feet, depth of 2.50 feet and length of 120 feet with smooth sides and bottom. In all these runs, the distribution of the bed shear stress τ_b and wall shear stress τ_w and centerplane velocity distribution were obtained whereas only in some of the runs detailed velocity distributions were obtained. Due to certain difficulties with the orifice-meter, the discharge was not directly measured and in the experiments with detailed velocity measurements, it was computed by graphical integration. The aspect ratio b/y_0 was varied from 6.79 to 20.28.

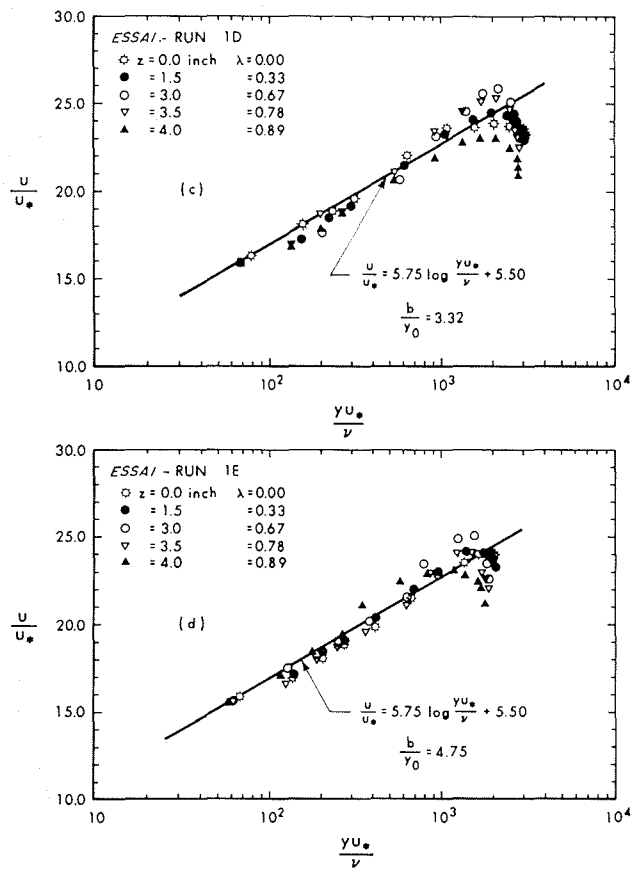

3 a/

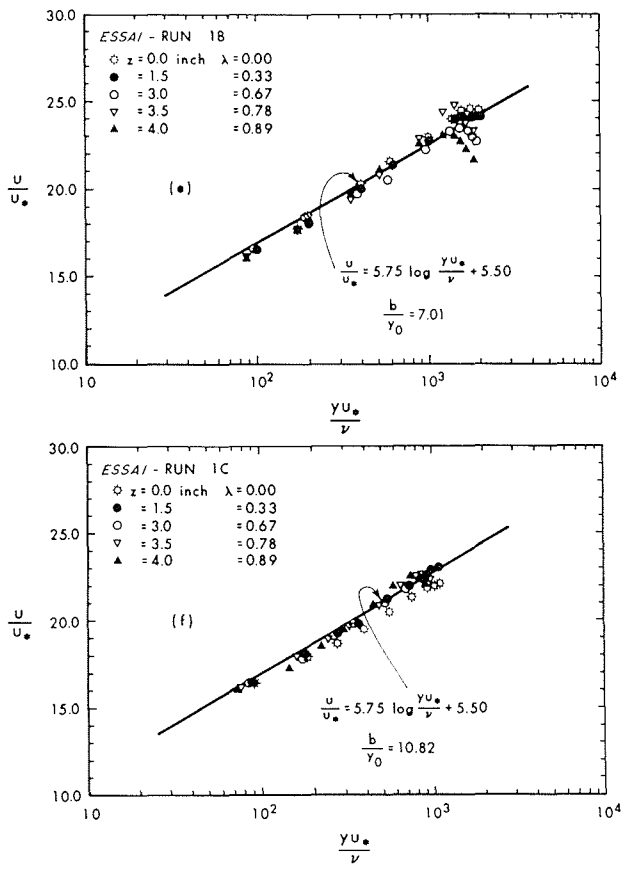

3 b/

The basic experimental data for all the three series are given in Table 1. In Table 1, S_0 is the slope of the channel, γ is the specific weight of water and υ is its coefficient of kinematic viscosity. U is the maximum velocity in the centerplane. In the run 3 T, τ_b was measured for the full bed width and τ_w was measured on both the side walls and the results were the same for either side of the centerplane.

Velocity distribution

The velocity distribution obtained on the centerline of the channel (ie. $\lambda = 0$) as well as for sections with non-zero values of λ were plotted with u/u_* versus log (yu_*/υ) where u_* is the shear velocity, equal to $\sqrt{\tau_b/\rho}$, at the foot of the corresponding normal line, and ρ is the mass density of water. A few typical plots are shown in Figure 3 for the aspect ratio b/y_0 equal to 0.83, 1.58, 3.32, 4.75, 7.01 and 10.82 respectively. From Figure 3 and the other related plots, it was found that the velocity distribution agrees well with the well known Karman-Prandtl equation [14]:

$$\frac{u}{u_*} = 5.75 \log \frac{yu_*}{\upsilon} + 5.50 \qquad (1)$$

even for values of λ as large as 0.89. It was also noticed that near the free-surface there is a dip in the velocity profile.

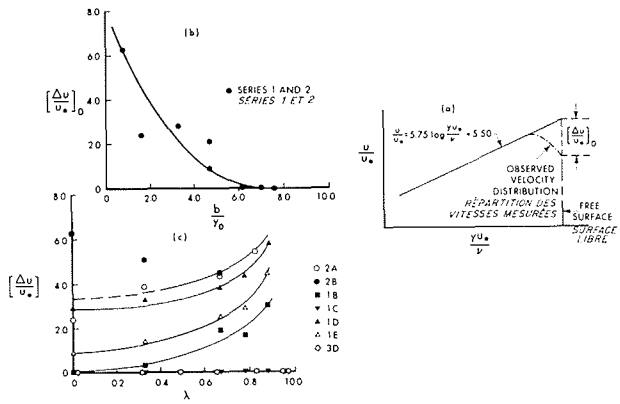

4/ Velocity dip at the free surface.
Chute de vitesse à la surface libre.

Concerning the dip in the velocity profile, it is generally believed that it is more due to the presence of secondary currents rather than the air drag [15, 16]. In this paper, without going into a discussion of these above two causes, a preliminary method is suggested for correlating the dip in the velocity at the free surface with the aspect ratio.

With reference to Figure 4 *a*, let $(\Delta u)_0$ be the difference between the actual velocity and that given by Eq. (1) at the free surface. It should be mentioned that in this investigation, the Pitot tube was placed as close as possible to the free-surface and the surface velocity was obtained by a small extra-

polation of the measured velocity profile. In a few cases, this predicted value of surface velocity was checked and found to agree with the observations on small surface floats. If $[(\Delta u)/u_*]_0$ is the dimensionless velocity dip at the free-surface, its variation with b/y_0 is shown in Figure 4 *b* for the first and second series. It is seen that $[(\Delta u)/u_*]_0$ decreases rapidly from about 6.0 at $b/y_0 = 1.0$ to zero at an aspect ratio of about 7.0. The experiments in the bigger channel did not show any appreciable value for $[(\Delta u)/u_*]_0$.

Further the experiments in the smaller channel showed that for any given experiment with an aspect ratio less than about 7.0, the dimensionless velocity dip at the surface $[(\Delta u)/u_*]$ increases as the side wall is approached. This effect is shown in Figure 4 *c*. Only the experiment with the smallest aspect ratio shows an opposite trend. It is not known definitely as to whether this reversal at small aspect ratios is due to the change in the pattern of the secondary currents.

Considering the side wall, taking the portion on which τ_w was essentially constant, if z' is the normal distance from the wall, the velocity distribution normal to the wall is studied in Figure 5 by plotting u/u_* versus log $(z'u_*)/\upsilon$ where $u_* = \sqrt{\tau_w/\rho}$. It is interesting to find that the data for the first series agree well with the Karman-Prandtl equation. Data of the other experiments also gave the same results.

Maximum bed shear stress

If τ_{bm} is the maximum value of the bed shear stress, occurring at the center of the channel, for channels of very large aspect ratio, τ_{bm} should be equal to $\gamma y_0 S_0$. The variation of $\tau_{bm}/\gamma y_0 S_0$ with the aspect ratio is studied in Figure 6 using the present experimental results along with those of Cruff. Even though there is some scatter, a mean curve could be drawn, which increases from about 0.3 at $b/y_0 = 1.0$ to unity at $b/y_0 \simeq 15$. Hence for the centerline bed shear stress to be equal to $\gamma y_0 S_0$, the aspect ratio should be greater than about 15.

Considering a rectangular channel of large aspect ratio with an uniform depth of y_0, at least the centerplane flow could be considered as a turbulent boundary layer of a thickness $\delta = y_0$. It is a fully grown boundary layer and the channel bed is under constant pressure. If U is the maximum observed velocity in the centerplane, then U corresponds to the free stream velocity of the boundary layer. A skin-friction coefficient c_{fb} is defined in the conventional manner:

$$c_{fb} = \frac{\tau_{bm}}{\rho U^2/2} \qquad (2)$$

For the plane turbulent boundary layer growing under constant pressure, on a flat plate the skin-friction coefficient has been given by a number of investigators. The relation given by Clauser [17] can be written as:

$$\sqrt{\frac{1}{c_f}} = 3.96 \log \left[\frac{U\delta}{\upsilon}\sqrt{c_f}\right] + 4.15 \qquad (3)$$

Karman [18] gave the equation for c_f with pipe flow constants as:

$$\sqrt{\frac{1}{c_f}} = 4.15 \log \left[\frac{U\delta}{\upsilon}\sqrt{c_f}\right] + 3.60 \qquad (4)$$

Eqs. (3) and (4) are shown plotted in Figure 7. The experimental results for c_{fb} are plotted in Figure 7 and they are somewhat higher than the Clauser and Karman curves. Further comments on this comparison will be made later after analysing the maximum shear stress on the side walls.

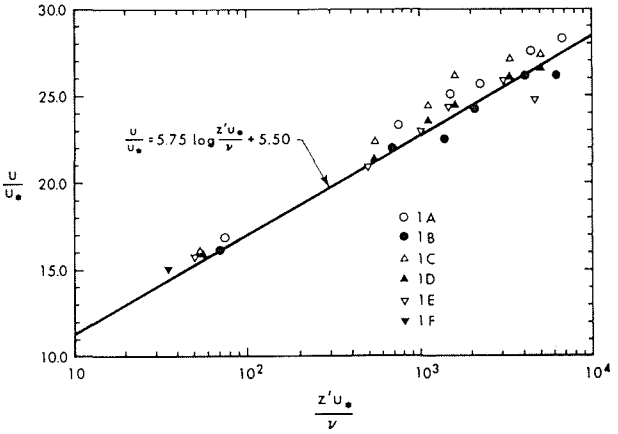

5/ Velocity distribution in the side wall boundary layer. *Répartition des vitesses dans la couche limite de la paroi latérale.*

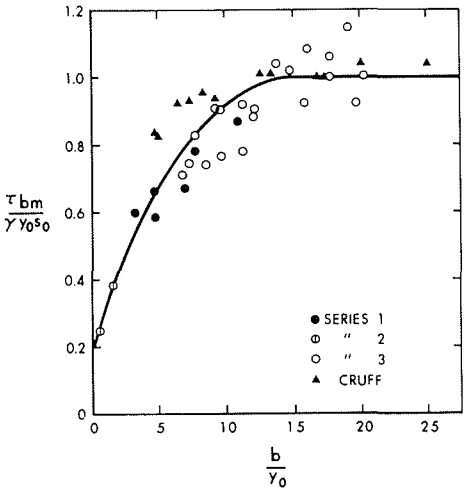

6/ Study of the maximum bed shear stress. *Etude de la contrainte de cisaillement maximale au fond.*

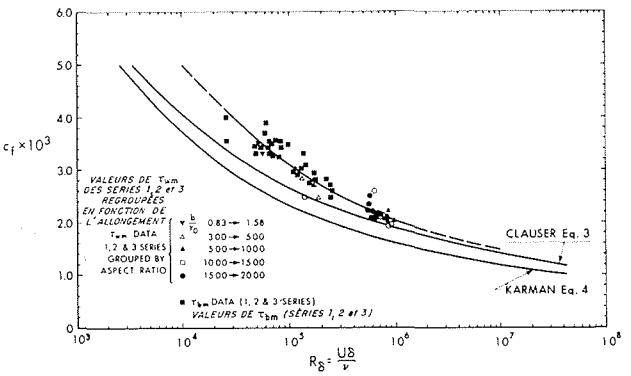

7/ Skin friction coefficient of the bed and side wall. *Coefficient de frottement superficiel sur le fond et la paroi latérale.*

Maximum side wall shear stress

Considering a rectangular channel of small aspect ratio, leaving a small layer near the bed, the flow could be imagined to be made of two fully-grown boundary layers of thickness $\delta = b/2$ on the side walls. Defining the skin friction coefficient c_{fw} as:

$$c_{fw} = \frac{\tau_{wm}}{\rho U^2/2} \qquad (5)$$

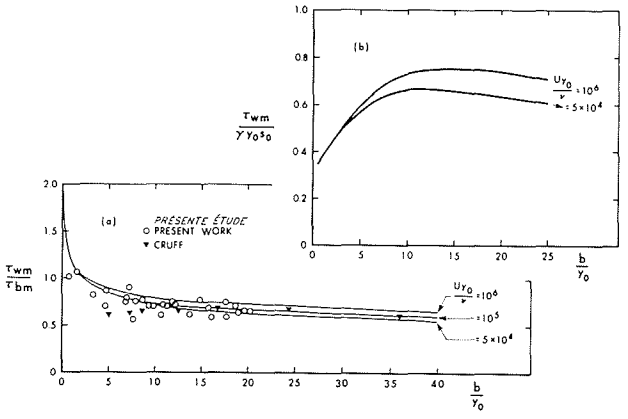

8/ Study of the maximum bed and side wall shear stress. *Etude de la contrainte de cisaillement maximale sur le fond et en paroi latérale.*

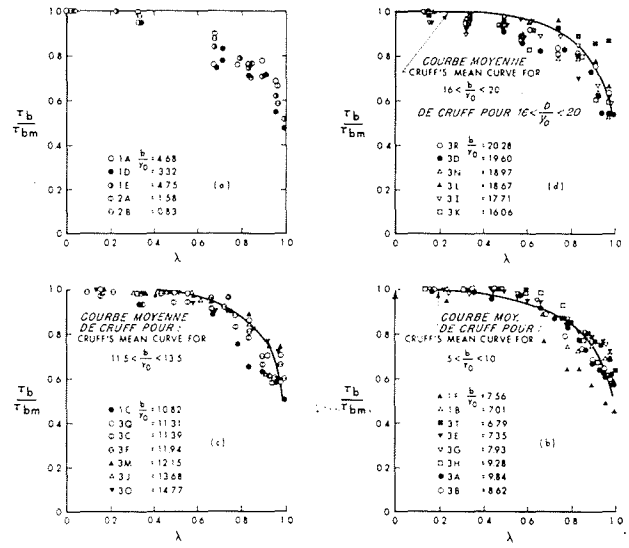

9/ Bed shear stress distribution. *Répartition de la contrainte de cisaillement sur le fond.*

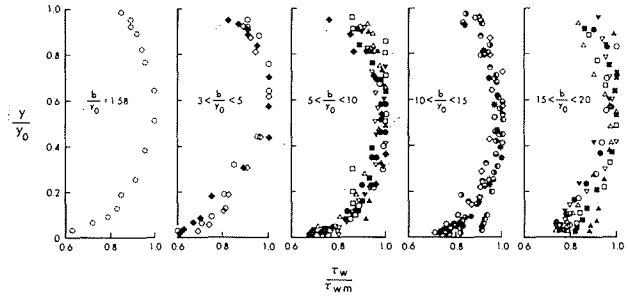

10/ Side wall shear stress distribution. *Répartition de la contrainte de cisaillement en paroi latérale.*

where U is the maximum centerplane velocity, the variation of c_{fw} with $\mathcal{R}_\delta = (Ub/2\upsilon)$ is shown in Figure 7. The data for c_{fw} varies in the same manner as c_{fb}, thereby showing that the bed boundary layer and side wall boundary layers are all governed by the general flat plate turbulent boundary layer theory. A curve is drawn through the experimental points and this curve could be expressed by the equation:

$$\sqrt{\frac{1}{c_f}} = 4.4 \log \left[\frac{\upsilon}{U\delta} \sqrt{c_f} \right] + 1.60 \qquad (6)$$

in which, for the bed boundary layer $c_f = c_{fb}$ and $\delta = y_0$ and for the side wall boundary layer $c_f = c_{fw}$ and $\delta = b/2$. The interaction of the bed and side boundary layers results in a variation of the bed as well as wall shear stresses which is considered in a later section.

Relation between τ_{bm} and τ_{wm}

It is possible to establish a relation between τ_{bm} and τ_{wm} and the aspect ratio of the channel. One could write:

$$\frac{\tau_{wm}}{\tau_{bm}} = \frac{c_{fw}}{c_{fb}} \qquad (7)$$

If:

$$\mathcal{R} = \frac{Uy_0}{\upsilon}$$

$$\sqrt{\frac{1}{c_{fw}}} = 4.4 \log \left[\frac{\mathcal{R}}{2} \frac{b}{y_0} \sqrt{c_{fw}} \right] + 1.60 \qquad (8)$$

$$\sqrt{\frac{1}{c_{fb}}} = 4.4 \log \left[\mathcal{R} \sqrt{c_{fb}} \right] + 1.60 \qquad (9)$$

Using Eqns. (7) to (9), it could be shown that :

$$\frac{\tau_{wm}}{\tau_{bm}} = f \left[\frac{b}{y_0}, \quad \mathcal{R} = \frac{Uy_0}{\upsilon} \right] \qquad (10)$$

Eq. (10) was evaluated for three values of $\mathcal{R} = 5 \times 10^4$, 10^5 and 10^6 and the variation of τ_{wm}/τ_{bm} with b/y_0 for these three Reynolds numbers is shown in Figure 8 *a*. It is seen that in the range of Reynolds number considered (which is typical of laboratory investigations) the effect of $\mathcal{R}$ is negligible only for b/y_0 less than about three. The experimental results of the authors as well as those of Cruff shown in Figure 8 *a*, agree generally well with the above calculations. For the range of $\mathcal{R}$ between 5×10^4 and 10^6 using the results of Figure 6 and Figure 8 *a*, the variation of $\tau_{wm}/\gamma y_0 S_0$ with b/y_0 was computed and the results are shown in Figure 8 *b*. It is interesting to see that for b/y_0 greater than about three the effect of the variation of the Reynolds number is appreciable.

Bed and side wall shear stress distributions

Typical variation of τ_b and τ_w have been shown in Figure 2. An attempt was made to give these distributions in groups, each for a certain range of the aspect ratio. This is done in Figure 9 and 10.

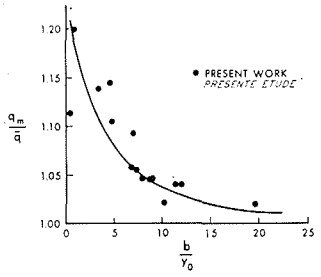

11/ Distribution of the discharge intensity.
Répartition de l'intensité du débit.

Table 1
Basic experimental data

Expt. No.	b (ft)	S_0	y_0 (ft)	b/y_0	Q (cfs)	τ_{bm} lbs/sq.ft.	$F_0 = \frac{V}{\sqrt{gy_0}}$	$\frac{U y_0}{\nu} \times 10^{-4}$	$\frac{Ub}{2\nu} \times 10^{-4}$	τ_{wm} lbs/sq.ft.
1A	0.75	0.0197	0.160	4.68	0.574	0.1155	2.10	8.05*	18.9	0.0810
1B	0.75	0.0197	0.107	7.01	0.344	0.0875	2.31	4.85	17.0	0.0720
1C	0.75	0.0197	0.069	10.82	0.172	0.0735	2.24	2.59	14.1	0.0450
1D	0.75	0.00656	0.226	3.32	0.574	0.0550	1.25	6.95	13.2	0.0450
1E	0.75	0.00656	0.158	4.75	0.344	0.0425	1.28	4.86	11.5	0.0370
1F	0.75	0.00656	0.099	7.56	0.172	0.0315	1.30	2.59	9.81	0.0180
2A	0.25	0.0193	0.158	1.58	0.143	0.0720	1.60	6.36	5.15	0.0763
2B	0.25	0.0193	0.301	0.83	0.330	0.0874	1.41	1.36	5.70	0.0880
3A	2.94	0.0096	0.289	9.84	5.472*	0.1344	2.11	17.6	89.3	0.0940
3B	2.94	0.0096	0.341	8.62	6.872*	0.1492	2.07	22.7	97.8	0.1160
3C	2.94	0.0096	0.258	11.39	4.664*	0.1236	2.13	15.2	87.1	0.0880
3D	2.94	0.0096	0.150	19.60	2.168*	0.0838	2.33	6.67	65.5	0.0550
3E	2.94	0.00636	0.400	7.35	7.128*	0.1126	1.69	23.8	87.9	0.1040
3F	2.94	0.00636	0.246	11.94	3.520*	0.0864	1.73	11.8	70.8	0.0650
3G	2.94	0.00636	0.371	7.93	6.496*	0.1233	1.72	21.6	85.5	0.0940
3H	2.94	0.00636	0.317	9.28	-	0.1138	-	17.3	80.3	0.0800
3I	2.94	0.00636	0.166	17.71	-	0.0738	-	6.65	59.0	0.0430
3J	2.94	0.00636	0.215	13.68	-	0.0887	-	9.55	65.6	0.0550
3K	2.94	0.00636	0.183	16.06	-	0.0802	-	7.67	61.6	0.0470
3L	2.94	0.00636	0.158	18.60	-	0.0781	-	6.24	58.1	0.0560
3M	2.94	0.00636	0.242	12.15	-	0.0864	-	11.6	70.9	0.0630
3N	2.94	0.00636	0.155	18.97	-	0.0710	-	5.96	56.5	0.0450
3O	2.94	0.00636	0.199	14.77	-	0.0806	-	8.54	63.2	0.0620
3P	2.94	0.00636	0.167	17.61	-	0.0706	-	6.71	59.3	0.0530
3Q	2.94	0.00636	0.260	11.31	-	0.0958	-	12.8	73.0	0.0690
3R	2.94	0.00636	0.145	20.28	-	0.0597	-	5.31	54.0	0.0390
3S	2.94	0.00636	0.187	15.72	-	0.0696	-	7.84	61.6	0.0480
3T	2.94	0.0058	0.433	6.79	7.16*	0.1100	1.506	24.4	82.8	0.0820

* Integrated discharge

Using Figure 9 it could be said in general that as the aspect ratio increases the bed shear stress distribution tends to become more uniform. There is considerable but no systematic scatter and the present data agree fairly well with the corresponding average curves of Cruff. Figure 9 *d* for b/y_0 16.1 to 20.0 exhibits some contradiction to the above general remark. Figure 10 shows the corresponding distributions for the side wall shear stress. Here it is even more difficult to discern clearly the effect of the aspect ratio.

Some supplementary results

If $\bar{q}$ is the average discharge intensity, equal to Q/b and q_m is the maximum discharge intensity, which was always found to occur on the centerplane, the ratio of q_m/q is plotted in Figure 11 against the aspect ratio b/y_0. It is interesting to see that for small values of b/y_0, q_m/q is much larger than unity. It could also be seen from Figure 11, tat as b/y_0 increases from 1.0 to 20, $q_m/\bar{q}$ decreases from about 1.20 to about 1.01.

Conclusions

Based on the experimental results for supercritical flows with the Froude number varying from 1.1 to about 2.4, the following conclusions could be drawn.

1. In the whole range of the aspect ratio studied, ie. 0.83 to about 20, the velocity distribution normal to the bed agrees well with the well known Karman-Prandtl logarithmic equation for values of λ up to about 0.89. The velocity distribution normal to the side walls also agrees with the same equation, but this aspect has not been extensively studied.

2. The maximum boundary shear stress on the bed and side walls has been correlated on the same basis as the flat plate constant pressure turbulent boundary layer. Some difference has been found to exist between the skin friction coefficient obtained in this work and that given by Clauser for the flat plate boundary layer.

3. It has been found that the ratio of the maximum side wall stress and the maximum bed shear stress varies with the aspect ratio as well as the Reynolds number. These remarks apply also to the ratio of the maximum wall shear stress and the maximum bed stress in an infinitely wide channel. The variation of the ratio of the maximum bed shear stress to that in an infinitely wide channel, with the aspect ratio has also been found. In addition, the distribution of the bed and wall shear stresses has also been obtained.

4. A preliminary analysis has been made regarding the dip in the velocity profile at the free surface.

Acknowledgements

The research work reported in this paper was done in the Civil Engineering Department of the University of Alberta, Edmonton. The authors are thankful to Mr. R. Tape for doing the experiments in the smaller channel. The authors are grateful to the National Research Council of Canada for the financial assistance provided.

Notations

The following symbols have been used in this paper:

b : breath of the rectangular channel, also suffix for bed;

c_f : coefficient of skin friction;

c_{fb} : skin friction coefficient, with respect to maximum bed stress;

c_{fw} : skin friction coefficient, with respect to maximum wall stress;

f : function;

$\mathcal{F}$: Froude number;

g : acceleration due to gravity;

q : discharge intensity;

$\overline{q}$: average discharge intensity;

q_m : maximum discharge intensity;

Q : discharge;

$\mathcal{R}$: Reynolds number $\left[= \frac{U y_0}{\upsilon}\right]$;

S_0 : bed slope;

u : point velocity;

u_* : shear velocity;

U : maximum centerplane velocity;

V : average velocity;

y : distance normal to the bed;

y_0 : normal depth of flow;

z : transverse distance from the centerplane;

z' : normal distance from the side wall;

γ : specific weight of water;

δ : boundary layer thickness;

λ : non-dimensional transverse distance;

υ : kinematic viscosity of water;

ρ : mass density of water;

τ_0 : boundary shear stress;

τ_b : bed shear stress;

τ_w : wall shear stress;

τ_{bm} : maximum value of τ_b;

τ_{wm} : maximum value of τ_w;

$\Delta u/u_*$: velocity dip at the free surface;

$[(\Delta u)/u_*]_0$: velocity dip at the free surface for the centre-plane.

References

[1] Leighly (J.B.). — Towards a theory of morphologic significance of turbulence in the flow of water in streams. *University of California, Publications in Geography*, vol. 6, No. 1, (1932).

[2] Lane (E.W.). — Some principles of design of stable channels in erodible material. *Proc. IAHR Congress*, India, 1951, p. 463-479.

[3] Lane (E.W.) — Design of stable channels. *Trans. American Soc. of Civil Engineers*, vol. 120, (1955), p. 1234-1279.

[4] Lundgren (H.) and Jonsson (I.G.). — Shear and velocity distribution in shallow channels. *Proc. American Soc. of Civil Engineers, J. of the Hyd. Div.*, (Jan. 1964), p. 1-21.

[5] Ippen (A.T.) and Drinker (P.A.). — Boundary shear stresses in curved trapezoidal channels. *Proc. American Soc. of Civil Engineers, J. of the Hyd. Division* (Sept. 1962).

[6] Preston (J.H.). — The determination of turbulent skin friction by means of Pitot tubes, *J. of the Royal Aero. Soc.*, (Feb. 1954), p. 109-121.

[7] Enger (P.F.). — Tractive force fluctuations around an open channel perimeter as determined from point velocity measurements. Paper presented at American Soc. of Civil Engineers convention at Phoenix (April 10-14, 1961).

[8] Cruff (R.W.). — Cross-channel transfer of linear momentum in smooth rectangular channels. *U.S. Geological Survey*, Water Supply Paper, 1592-B, (1965).

[9] Replogle (J.A.) and Chow (V.T.). — Tractive-force distribution in open channels. *Proc. American Soc. of Civil Engineers, J. of the Hyd. Div.* (March 1966), p. 169-191.

[10] Davidian (J.) and Cahal (D.I.). — Distribution of shear in rectangular channels. *U.S. Geological Survey*, Professional Paper 475-C, (1963), p. C206-C208.

[11] Rouse (H.). — Critical analysis of open-channel resistance. *Proc. American Soc. of Civil Engineers, J. of the Hyd. Div.*, (July 1965), p. 1-25.

[12] Rajaratnam (N.). — Preston tube with a hemispherical nose. *Civil Engineering and Public Works Review*, (Nov. 1965), p. 1642.

[13] Rajaratnam (N.) and Muralidhar (D.). — Prandtl tube as Preston tube. *Civil Engineering and Public Works Review*, (May 1968), p. 542.

[14] Schlichting (H.). — Boundary-Layer Theroy, English Translation published by *McGraw-Hill Book Co. Inc.*, New York, (1955).

[15] Chow (V.T.). — Open Channel Hydraulics, *McGraw Hill Book Co. Inc.*, (1959), p. 24-25.

[16] Kennedy (R.J.) and Fulton (J.F.). — The effect of secondary currents upon the capacity of a straight open channel. *Trans. Eng'rg. Inst. of Canada*, vol. 5, No. 1, (1961), p. 12-18. [This reference gives an extensive list of other investigations on secondary currents in channels].

[17] Clauser (F.H.). — The turbulent boundary layer. Adv. in Applied Mech., vol. 4, *Academic Press*, New York, (1956).

[18] Schubauer (G.B.). and Tchen (C.M.). — Turbulent Flow, No. 9, Princeton Aeronautical Paperbacks, *Princeton University Press*, (1961).